Suppression of spatiotemporal chaos in the oscillatory CO oxidation on Pt(110) by focused laser light

Christian Punckt*
Department of Physical Chemistry, Fritz Haber Institute of the Max Planck Society, Faradayweg 4-6, 14195 Berlin, Germany

Michael Stich†
Instituto Pluridisciplinar, Universidad Complutense de Madrid, Paseo Juan XXIII 1, 28040 Madrid, Spain

Carsten Beta
Institute of Physics and Astronomy, University of Potsdam, Karl-Liebknecht-Str. 24/25, 14476 Potsdam-Golm, Germany

Harm Hinrich Rotermund
Department of Physics and Atmospheric Science, Dalhousie University, Halifax, Canada NS B3H 3J5
(Received 15 October 2007; published 30 April 2008)

Chemical turbulence in the oscillatory catalytic CO oxidation on Pt(110) is suppressed by means of focused laser light. The laser locally heats the platinum surface which leads to a local increase of the oscillation frequency, and to the formation of a pacemaker which emits target waves. These waves slowly entrain the medium and suppress the spatiotemporal chaos present in the absence of laser light. Our experimental results are confirmed by a detailed numerical analysis of one- and two-dimensional media using the Krischer-Eiswirth-Ertl model for CO oxidation on Pt(110). Different control regimes are identified and the dispersion relation of the system is determined using the pacemaker as an externally tunable wave source.

DOI: 10.1103/PhysRevE.77.046222 PACS number(s): 05.45.Gg, 82.40.Bj, 82.40.Np

I. INTRODUCTION

Spontaneously emerging dissipative structures are a hallmark of dynamical systems far from thermodynamic equilibrium [1]. Self-organizing structures arise in such systems as a consequence of the underlying nonlinear dynamics. A lot of research in this field is focused on low-dimensional systems and complex behavior in the time domain such as oscillations and deterministic chaos [2]. In parallel, research efforts also consider pattern formation in high-dimensional, spatially extended nonequilibrium systems [3]. Besides the classical hydrodynamic instabilities, systems of the reaction-diffusion type are among the most widely studied examples [4]. In spite of large progress, major problems remain unresolved, such as the theory and description of spatiotemporal chaos, which stimulates ongoing research in this open and active field.

Similar phenomena of self-organization can be often observed in dynamical systems of very different microscopic nature. In such cases, the underlying equations can be reduced to coarse-grained descriptions that belong to the same overall category of dynamical behavior [5]. Excitability, for example, can be encountered in nerve cells, as well as in chemical reactions, cardiac tissue, and population dynamics [6]. For this reason, spatiotemporal pattern formation is commonly studied in well-established laboratory systems since the results obtained from such laboratory models can be used to understand the behavior of a whole class of dynamical systems. The classical laboratory setup to study pattern formation in chemical systems is the Belousov-Zhabotinsky (BZ) reaction [7], the homogeneously catalyzed oxidation of malonic acid by bromate. Improvements in the experimental setup, in particular the introduction of continuously fed open gel reactors [8], have greatly widened the range of accessible phenomena that can be studied in this system.

Besides reactions in aqueous phase, a set of heterogeneous catalytic surface reactions has been established as a laboratory system to study pattern formation in two-dimensional reaction-diffusion systems [9,10]. The most prominent example among these reactions is the catalytic CO oxidation on Pt(110) which shows a rich variety of spatiotemporal concentration patterns including traveling pulses, standing waves, and target patterns as well as spiral waves and chemical turbulence [11]. While the reaction scheme of the BZ system is complex, the mechanism of the catalytic CO oxidation is relatively simple and each elementary step has been individually studied using surface scientific diagnostics [12]. A three-variable kinetic reaction model was designed that has been successfully applied to describe most of the experimentally observed dynamical features [13].

In recent years, research interests have shifted from analyzing and understanding the spontaneously emerging spatiotemporal patterns to actively influencing and manipulating the formation of structures in dynamical systems [14]. Efforts were made to guide self-assembly with the goal of finding new engineering paradigms for the design of complex nonequilibrium structures [15]. Extensions and refinements of the classical laboratory systems have set the stage for research on the fundamental aspects of this topic. For both

*Current address: Department of Chemical Engineering, Princeton University, Princeton, NJ 08544; cpunckt@princeton.edu

†Current address: Centro de Astrobiología (CSIC-INTA), Instituto Nacional de Técnica Aeroespacial, Ctra de Ajalvir km. 4, 28850 Torrejón de Ardoz, Madrid, Spain.

the BZ reaction and the catalytic oxidation of CO on platinum, modifications have been introduced that turn the system into an externally addressable active medium. For example, in the case of the BZ reaction, a light-sensitive variant was designed [16] that allows global as well as local control of the dynamics by illumination of the medium [17–19].

For the catalytic CO oxidation on Pt(110) the experimental setup has been extended such that the dynamics can be manipulated globally as well as locally. Global system parameters can be modulated by real-time control of partial pressures in the reactor. This approach has been extensively used to study pattern formation under global delayed feedback [20]. The stabilization of feedback-induced patterns has been investigated [21], as well as control and suppression of spatiotemporal chaos [22]. Also length-scale sensitive feedback schemes have been considered [23]. The experiments on feedback control were complemented by numerical simulations using a realistic reaction model [24,25] and by more general theoretical analysis in the framework of the complex Ginzburg-Landau equation (CGLE) [26–28]. Furthermore, global periodic forcing has been implemented to explore different subharmonic regimes of resonant pattern formation [29,30].

Besides global control, also local addressing of system dynamics could be implemented in the CO oxidation system. By means of a focused laser beam the kinetic parameters can be changed in a confined region via localized heating [31]. This approach has been successfully applied to initiate [32] and manipulate propagating reaction-diffusion waves [33], to enhance surface catalytic reactivity [34–36], to perform localized periodic forcing [37], and to induce target patterns [38]. The combination of dynamic local control by focused laser light and stationary microstructures gave new insights into the propagation behavior and stability of patterns in this system [39,40].

The high flexibility in applying global and local forces to the system opens up opportunities to experimentally explore new control strategies. In particular, control of spatiotemporal chaos is a field of intense research ranging from the fundamental sciences to engineering and medicine problems [41]. Besides the application of global forces, local stimulation seems a promising perspective to implement control schemes of low invasiveness that induce synchrony by applying only minimal perturbations. In a reaction-diffusion system, target patterns are the most obvious choice to transport the information of a localized control input, thereby exerting a nonlocal, synchronizing impact. They consist of concentric waves that are periodically emitted from a central pacemaker. Target patterns are ubiquitous spatiotemporal structures in reaction-diffusion systems and were already reported by Zaikin and Zhabotinsky in their classical paper on the BZ reaction [42]. Although they are mostly associated with local heterogeneities, also self-organized pacemakers and target patterns can emerge in uniform reaction-diffusion systems [43,44].

In a theoretical work, Jiang and co-workers have shown that spatiotemporal chaos can be controlled in the CGLE by a target pattern that grows and eventually entrains the entire medium [45]. Recently, chemical turbulence in the catalytic CO oxidation has been characterized [46] and could be described by similar dislocation dynamics as the disordered states in the CGLE. Furthermore, we have demonstrated in previous work that target patterns can be initiated in a highly controlled fashion in catalytic CO oxidation using a focused laser beam [38]. Together, these results prompted us to undertake a first investigation of turbulence control by artificially induced pacemakers that involves both experiments and numerical simulations. Preliminary results from this study have been recently presented in Ref. [47].

The paper is divided into an experimental and a theoretical part. First, we present the experimental setup and examples of how turbulent patterns can be suppressed by means of focused laser light in the experiment. It is analyzed how the degree of control varies when reaction parameters are changed. In the theoretical section, results from numerical simulations using the Krischer-Eiswirth-Ertl model for CO oxidation on Pt(110) [13] are presented. Detailed control diagrams are calculated which show the dependence between applied control signal and the response of the system. Also, the dispersion relation of laser-induced wave trains is determined.

II. EXPERIMENTAL SETUP AND RESULTS

Experiments are performed using a Pt(110) single crystal of 10 mm in diameter located in an ultrahigh-vacuum (UHV) chamber. For accurate control of the reaction parameters (temperature, CO and oxygen partial pressures), the chamber is equipped with a computer controlled gas dosing system, that allows for adjusting the partial pressures of CO and oxygen. The platinum sample is heated from the back with a halogen lamp. Reflection anisotropy microscopy (RAM) is used to image concentration patterns on the platinum surface. This method provides high spatial resolution (<10 μm), a large working distance (>10 cm) necessary for UHV applications, and sufficient sensitivity to visualize subtle changes of the crystal surface during the propagation of reaction patterns [48–50]. Images are taken with a video CCD camera at a rate of 25 images per second and stored on a DVD recorder. Local control of the surface reaction is achieved by focusing the light of an Ar-ion laser (wavelength 514 nm) onto the platinum surface. This creates a temperature heterogeneity on the catalyst which has a bumplike, almost Gaussian shape with a diameter of about 50 μm and an amplitude of 3 K for a laser power of $P_{\mathrm{Laser}}=50$ mW. Consequently, the reaction rate is locally increased, since several steps in the CO oxidation reaction are thermally activated. Stray light of this laser beam which is reflected into the imaging optics, is filtered out by means of an interference filter that allows only the wavelength of the imaging laser light (488 nm) to pass. Therefore, the laser spot is not visible in the images presented below. A sketch of the experimental setup is shown in Fig. 1.

Experiments are conducted in the following way: After cleaning the Pt crystal by repeated Ar-ion sputtering and annealing at 900 K, the sample heating is switched on, and light of the Ar-ion laser is focused onto the center of the sample, so that the temperature of the platinum crystal (T)

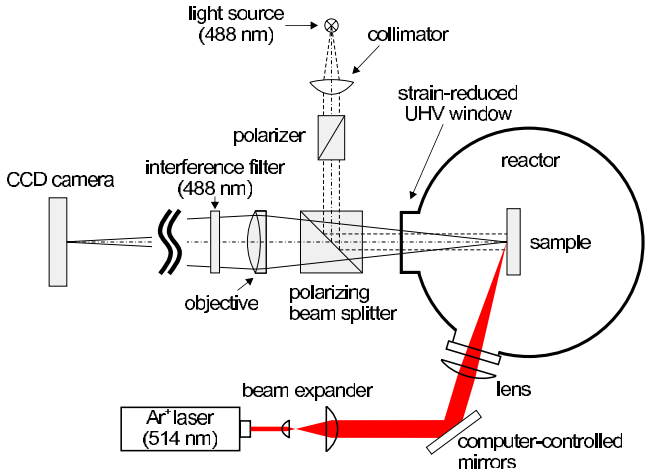

FIG. 1. (Color online) Experimental setup. Upon reflection at the platinum surface (sample) the light changes polarization because the Pt(110) surface is optically anisotropic. When covered with CO, the optical properties of the crystal surface change slightly compared to a clean or oxygen covered surface. This is visualized using the polarizing beam splitter cube which acts as a filter. Light reflected from reactive surface areas is blocked, but light reflected from surface regions covered with CO can pass. The platinum surface is imaged onto the chip of a CCD camera using a simple achromatic lens. The light of an Ar-ion laser is focused onto the surface and can be positioned via computer controlled mirrors. Reproduced from [50].

equilibrates at the desired value. The laser spot is then moved to the periphery of the sample. Since it not only influences the temperature locally but is also responsible for a global temperature increase of about 3 K, the laser must remain focused on the sample at all times. This is, because no active temperature control is used since the delay in a control loop would cause intolerable temperature fluctuations. The partial pressures of CO and oxygen (p_{CO} and p_{O_2}) are now adjusted in such a way, that turbulent oscillatory patterns can be observed. Then the laser spot is brought back to the center of the observed sample area. After a few seconds, a target pattern originating from the location of the laser spot starts to grow and eventually covers a large fraction of the observed area [Figs. 2(a)–2(c)].

This process can be understood by measuring the frequency at different locations on the surface. To this end, the recorded image sequence was stored on a computer and analyzed with MatLab. At selected points in the images the mean brightness in a 3×3 pixel area (corresponding to approximately 6×6 μm^2 on the platinum surface) was determined and stored. The time series was Fourier transformed within an 80 s time window at the beginning of the sequence. This corresponds to a frequency resolution of 0.0125 Hz. Figure 2(d) shows frequency spectra at the location of the laser spot (thick blue curve) and at points far away from the growing target pattern. The presence of the laser spot locally increases the frequency of oscillations by about 0.1 Hz. The growing phase difference between the oscillations at the laser focus and in the surrounding medium leads to the periodic emission of concentric waves at a rate of about one wave every 10 s. The laser spot has generated a pacemaker in the

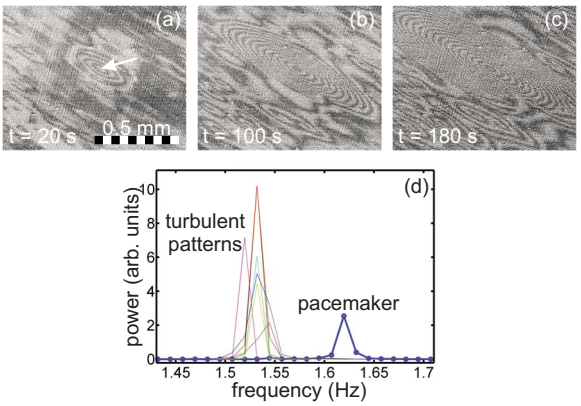

FIG. 2. (Color online) Suppression of turbulence by a laser induced target pattern. (a)–(c) Snapshots at indicated time moments after initiation of the laser spot. (d) Frequency spectrum at the center of the target pattern compared to frequency of the background dynamics. The white arrow in (a) indicates the position of the laser spot. The reaction parameters are $P_{Laser}=49$ mW, $p_{O_2}=1.84\times10^{-4}$ mbar, $p_{CO}=7.84\times10^{-5}$ mbar, and $T=538$ K.

system. Note that the elliptical shape of the target pattern is due to an anisotropy in CO diffusion on the Pt(110) surface.

Figure 3 illustrates what happens, when the laser spot is moved across the surface after a target pattern has already evolved. The frequency at the old (position 1) and the new (position 2) location of the laser spot is analyzed by calculating the fast Fourier transform (FFT) of the time evolution of the local gray value in 20 s time windows shifted in intervals of 10 s. The frequency values plotted in Fig. 3(c) are obtained by weighted averaging (with respect to the peak

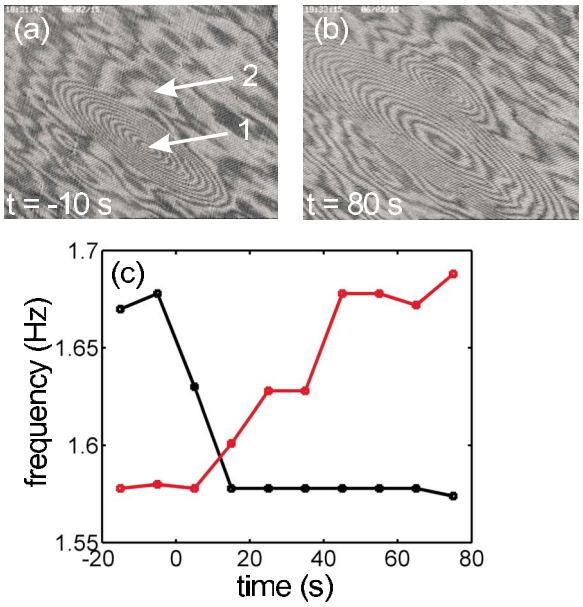

FIG. 3. (Color online) Moving the laser spot. (a) Snapshot 10 s prior to move, arrows indicate old (1) and new (2) position of the laser spot, (b) snapshot 80 s after move, (c) frequency evolution at the old (black) and the new (red) location of the laser spot. The reaction parameters are $P_{Laser}=53$ mW, $p_{O_2}=1.84\times10^{-4}$ mbar, $p_{CO}=7.84\times10^{-5}$ mbar, and $T=538$ K.

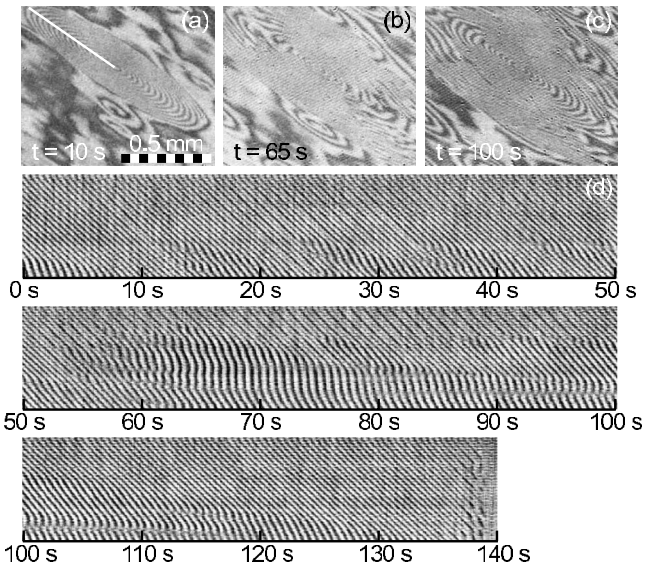

FIG. 4. Partial control. (a)–(c) Snapshots of the system at indicated time moments. (d) space-time plots along the line indicated in (a). After the oxygen pressure is decreased from 2.064×10^{-4} mbar to 2.058×10^{-4} mbar at $t=45$ s, the target pattern collapses via a cascade of phase slips. The reaction parameters are $P_{\mathrm{Laser}}=63$ mW, $p_{\mathrm{CO}}=8.40\times10^{-5}$ mbar, $T=539$ K, $p_{\mathrm{O}_2}=2.068\times10^{-4}$ mbar for $t>95$ s.

height) over the frequency spectrum close to the frequency peak. While at position 1 the frequency quickly drops to a value corresponding to the natural frequency of the system, at position 2 it increases slowly and reaches the value of the old pacemaker after 40 s. Despite the quick frequency drop, the old target pattern does not disappear instantaneously, but remains stable for more than 80 s. Its wavelength λ is slowly increasing, because the pattern must obey the dispersion relation of the system. While the wavelength for the laser induced 1.67 Hz oscillations is about $\lambda=50$ μm this value increases to $\lambda=90$ μm during the shown time interval after movement of the laser spot. From numerical results displayed below [Fig. 9(b)] it can be expected that a continuous phase diffusion process will asymptotically lead to a pattern with diverging wavelength, thus resembling uniform oscillations. However, since in the experiment uniform oscillations are unstable, the turbulent pattern outside the area covered by the diffusing target pattern will replace the regular wave pattern eventually.

The degree to which control can be achieved depends on a number of parameters such as laser power, spot size, and, of course, the reaction parameters. It is obvious that too little laser power will only have a negligible influence on the system frequency, and no control will be observed. But is there an upper limit for the laser power? In the experiment, the effect of varying laser power is difficult to study systematically because it not only changes the control force but also the global temperature of the system. Therefore, the dependence of control efficiency on the oxygen partial pressure was measured. In Fig. 4, an example of our experimental results is shown. In the beginning, the area heated by the laser spot emits a target pattern (a). Then, at $t=45$ s the oxygen partial pressure was slightly decreased. A few seconds later, a breakdown of the target pattern is observed (b). The oxygen pressure was readjusted to a higher value at $t=95$ s. Now the target pattern starts to grow again (c). A closer look at the space-time plots shown in Fig. 4(d) reveals, that the collapse of the target pattern occurs through a number of phase slips. A similar effect has been observed in theoretical studies of the complex Ginzburg-Landau equation [51]. Here, the emergence of phase slips has been attributed to the large difference between the natural frequency of the system and the frequency of the pacemaker. The surrounding medium is unable to follow the rapid oscillations of the wave source.

An analysis of the frequencies along the longer axis of the target pattern illustrates this process. Since we need a high temporal resolution we calculate the FFT in a 20 s window which is moved along the time axis in steps of 0.2 s. This gives an estimate of the change in local oscillation frequency over time. In a second step, these frequency values are used as initial conditions for an algorithm which fits sine functions to the data within 3 s time windows, for which an FFT-based algorithm would not provide sufficient resolution in frequency space. Figure 5 shows the frequencies at selected locations. It can be seen that in the beginning ($t<50$ s) up to a distance of 10 λ from the position of the laser spot, the system oscillates at the same frequency as the pacemaker. When the oxygen pressure is decreased, the natural frequency of the system drops from 1.52 Hz to 1.47 Hz while the pacemaker maintains a constant frequency. Thus, the difference between the pacemaker frequency and the natural system frequency is increased. During the following seconds, the frequencies at distances between 4λ and 10λ begin to fluctuate. This is caused by the phase slips occurring in this region [compare Fig. 4(d)]. Further away from the pacemaker, the fluctuations stop and the frequencies reach the level of the natural frequency [see Fig. 5(b)]. When the oxygen pressure is increased again, the growth of the target pattern can be identified in the frequency diagram. In perfect order, the frequency curves for different distances approach the pacemaker frequency, beginning with the locations in the vicinity of the pacemaker, until eventually (at $t=130$ s) also at a distance of 14 λ the pacemaker frequency is measured.

To summarize, by locally increasing the frequency of oscillations we are able to generate a pacemaker in the system which emits a target pattern and suppresses chemical turbulence. Target patterns remain visible for some time after the laser spot is moved to another location on the sample although the wavelength of the pattern increases due to a phase diffusion process. If the frequency difference between the pacemaker and the turbulent pattern becomes too large, control of a large system area is no longer possible, because the system is unable to follow the fast oscillations of the pacemaker and phase slips occur.

III. MODEL AND SIMULATIONS

In this section, we first introduce a model which describes the spatiotemporal dynamics of the CO oxidation reaction on Pt(110), the Krischer-Eiswirth-Ertl (KEE) model [13]. Then, we present the central result of the numerical simulations,

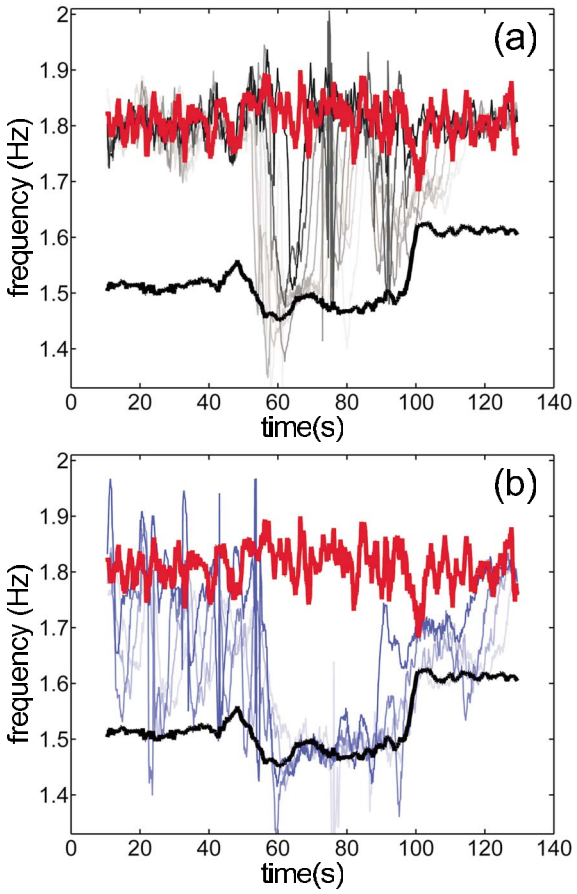

FIG. 5. (Color online) Frequency analysis of the data shown in Fig. 4. (a) Thick red curve, frequency of the pacemaker; thick black curve, frequency far away from the target pattern (natural frequency), the curves in different shades of gray indicate the frequency at distances of 4λ (dark gray) to 10λ (light gray) from the pacemaker along the white line in Fig. 4(a). (b) Blue lines indicate the frequency at distances of 11λ (dark blue) to 14λ (light blue) from the pacemaker.

i.e., the suppression of turbulence through the application of a temperature heterogeneity (pacemaker). We present control diagrams where we distinguish between different control regimes, show for which partial pressures of CO and oxygen control can be achieved, and give dispersion relations. Results for one- and two-dimensional media are shown. The creation of target patterns by heterogeneities in the KEE model under nonturbulent conditions has been presented in [38] and preliminary results for turbulence suppression in one dimension have been shown in [47].

A. Turbulence and temperature heterogeneities in the Krischer-Eiswirth-Ertl model

The KEE model consists of a system of three coupled partial differential equations,

$$\partial_t u = k_1 s_{\mathrm{CO}} p_{\mathrm{CO}}(1-u^3) - k_2 u - k_3 uv + D\nabla^2 u, \tag{1}$$

$$\partial_t v = k_4 p_{\mathrm{O}_2}[s_{\mathrm{O},1\times1} w + s_{\mathrm{O},1\times2}(1-w)](1-u-v)^2 - k_3 uv, \tag{2}$$

TABLE I. Parameters used for numerical simulations.

k_1	3.14×10^5 s^{-1} mbar^{-1}	Impingement rate of CO
k_2	$=\nu_2 \exp(-E_2/k_BT)$	Desorption rate of CO
ν_2	2×10^{16} s^{-1}	
E_2	38 kcal mol^{-1}	
k_3	$=\nu_3 \exp(-E_3/k_BT)$	Reaction rate
ν_3	3×10^6 s^{-1}	
E_3	10 kcal mol^{-1}	
k_4	5.86×10^5 s^{-1} mbar^{-1}	Impingement rate of O_2
k_5	$=\nu_5 \exp(-E_5/k_BT)$	Phase transition rate
ν_5	1056.1 s^{-1}	
E_5	7 kcal mol^{-1}	
s_{CO}	1.0	CO sticking coefficient
$s_{\mathrm{O},1\times1}$	0.6	Oxygen sticking coefficient on the 1×1 phase
$s_{\mathrm{O},1\times2}$	0.4	Oxygen sticking coefficient on the 1×2 phase
$u_0, \delta u$	0.35, 0.05	Parameters for the structural phase transition
D	$=D_0 \exp(-E_D/k_BT)$	CO diffusion coefficient
D_0	3.56×10^6 μm^2 s^{-1}	
E_D	12.3 kcal mol^{-1}	

$$\partial_t w = k_5\left\{\left[1+\exp\left(\frac{u_0-u}{\delta u}\right)\right]^{-1} - w\right\}, \tag{3}$$

where the variables u, v, and w are normalized between 0 and 1 and represent the CO coverage, the oxygen coverage, and the fraction of the surface found in the nonreconstructed 1×1 phase, respectively. Adsorption of CO and oxygen on the catalyst surface, desorption and surface diffusion of CO, as well as reaction between the two adsorbed species are taken into account. Oxygen desorption and diffusion are negligible for the considered temperature ranges. The diffusion constant of CO is assumed to be independent of the system state.

The temperature dependence of the rate constants of CO desorption, CO diffusion, surface reaction, and surface structural phase transition is assumed to follow a simple Arrhenius-type relation, $k_i=\nu_i \exp(-E_i/k_BT)$. Rate constants and activation energies are given in Table I.

For the chosen parameter set, in particular, base temperature $T_0=543.5$ K (constant throughout this work) and partial pressures of CO and O_2, $p_{\mathrm{CO}}=4.46\times10^{-5}$ mbar and $p_{\mathrm{O}_2}=1.1\times10^{-4}$ mbar, the system displays spatiotemporally chaotic states of intermittent turbulence, characterized by propagating defects that form and annihilate in cascades, and hence by the alternation of intervals with many interacting wave fragments and regimes of relative regularity [25]. In Fig. 6(a) we show an example for such a situation: Starting from an initial condition representing locally perturbed uniform oscillations, we observe how in a short time a regime of disordered waves emerges. Note that no heterogeneity is present there. Spatiotemporal disorder is created in a similar

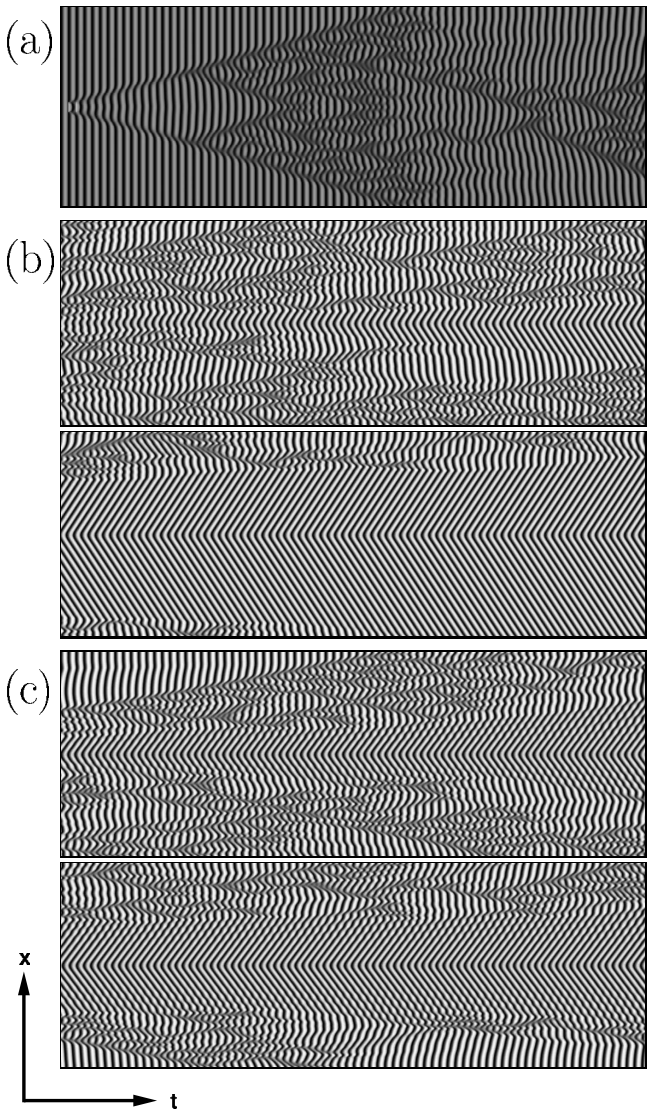

FIG. 6. Spatiotemporal dynamics in the KEE model. Parameters: $T_0=543.5$ K, $p_{CO}=4.46\times10^{-5}$ mbar, and $p_{O_2}=1.1\times10^{-4}$ mbar. Shown are space-time diagrams in gray scale for u. Black (white) denotes minimum (maximum) values of u in the shown simulation. (a) Development of intermittent turbulence from an initial perturbation (strong, momentary, localized increase of u in the center of the medium). System size is $L=800$ μm, shown time interval $t=[0,200]$ s. (b) Complete control: Full suppression of turbulence by a heterogeneous pacemaker ($\Delta T=0.13$ K, $\sigma=16$ μm). System size is $L=1400$ μm, heterogeneity is switched on at $t=0$ s. Shown are time intervals $t=[200,400]$ s (upper panel) and $t=[839,1039]$ s (lower panel). (c) Partial control: Spatially confined suppression of turbulence by a heterogeneous pacemaker ($\Delta T=0.17$ K, $\sigma=16$ μm). System size is $L=1400$ μm, heterogeneity is switched on at $t=0$ s. Shown are time intervals $t=[200,400]$ s (upper panel) and $t=[1300,1500]$ s (lower panel).

way as in the excitable regime of the CO oxidation reaction where the backfiring instability of traveling waves induces turbulence [52]. Uniform oscillations are linearly stable, i.e., small perturbations decay. However, turbulence develops from most initial conditions—in particular from random ones—and persists for large system size. Intermittent turbulence and the back-firing instability are interesting topics in their own right (see Refs. [53–58]) and a thorough discussion is beyond the scope of this paper. For a probabilistic description of defect-mediated turbulence in the CO oxidation system, see Ref. [46].

The impact of the laser on the reaction is modeled by a local increase in surface temperature with Gaussian profile

$$T(x) = T_0 + \Delta T \exp[-(x-x_0)^2/(2\sigma^2)]. \tag{4}$$

The center of the profile is chosen to coincide with the center of the medium, unless stated otherwise. The temperature increase affects the dynamics indirectly through a local change of the above-mentioned rate constants k_2, k_3, k_5, and D. The usage of a Gaussian profile is justified by earlier investigations presented elsewhere [31,35], where the temperature profile induced by the laser spot was measured and different theoretical approximations where compared.

The KEE model was integrated numerically on one-dimensional (1D) and two-dimensional (2D) spatial domains using a forward-Euler scheme and a nearest-neighbor representation of the Laplacian operator. No-flux and periodic boundary conditions were used in 1D, no-flux in 2D. The fundamental pattern-forming process, the creation of target waves at a heterogeneity, does not depend on the choice of the boundary condition. For the one-dimensional simulations, the system length is $L=800$ μm, the grid size $\Delta x=4$ μm, and the time step $\Delta t=0.001$ s.

For the two-dimensional simulations, the system dimensions are $L_x=L_y=800$ μm. The grid size of $\Delta x=\Delta y=4$ μm as well as the time step $\Delta t=0.001$ s are maintained. For the temperature heterogeneity again a Gaussian profile is assumed,

$$T(x,y) = T_0 + \Delta T \exp\left(-\frac{(x-x_0)^2+(y-y_0)^2}{2\sigma^2}\right), \tag{5}$$

located in the center of the computational domain at $(x_0,y_0)=(400\ \mu\text{m},400\ \mu\text{m})$. The anisotropy of CO diffusion on the Pt(110) surface results in a simple rescaling of the patterns (target patterns are elliptic and not circular) and is therefore neglected in the model calculations.

B. Control of turbulence in one-dimensional media

In this section, we demonstrate the fundamental effect of a pacemaker, i.e., how a temperature heterogeneity of appropriate size and temperature shift can create target waves that are able to suppress turbulence. Two cases of control of turbulence can be distinguished: Complete control, where target waves eventually fill the whole system, and partial control, where target patterns are only observed in the vicinity of the temperature spot.

A temperature heterogeneity in the catalytic CO oxidation system can create target waves, as shown, both for theory and experiment in Ref. [38]. In the oscillatory regime, a local temperature increase leads to a local frequency increase, as also shown in Sec. II. That such a frequency increase is able to create waves capable of suppressing turbulence is shown in Fig. 6(b). In this section, we fix the partial pressures as $p_{CO}=4.46\times10^{-5}$ mbar, and $p_{O_2}=1.1\times10^{-4}$ mbar. As initial

condition, we have chosen a state of intermittent turbulence. We see in the space-time plot that at the location of the laser spot waves are created. After a transient during which the waves annihilate with wave fragments of the underlying turbulence, waves are able to propagate further and finally fill the whole medium, thus establishing complete control.

Partial control describes the case where turbulence in the system is only suppressed in a spatially confined region around the temperature heterogeneity. In Fig. 6(c), we show a corresponding simulation where we dropped a part of the initial transient: In an area comprised of approximately 2 to 3 wavelengths around the heterogeneity, regular target waves are present. In the transition area, these waves decay and in the far-field, native turbulence is observed. A detailed inspection of the waves reveal that they are increasingly modulated as they travel outwards, until they disappear in a phase slip or annihilate through collision with the wave fragments of the spatiotemporally chaotic patterns. This scenario resembles closely not only the experimental results shown in Sec. II, but also the behavior of Eckhaus-unstable traveling waves created by a heterogeneity in the CGLE [51,59]. Hence, we can infer that the mechanism leading to this effect is analogous to the Eckhaus instability of traveling waves in the CGLE. More arguments supporting this interpretation are presented below.

In Fig. 7(a) we show the different spatiotemporal regimes that are found as we vary the size and the temperature shift of the heterogeneity. This diagram has been obtained for simulation times of 3000 s (close to the boundaries of the regimes up to 6000 s), with the heterogeneity located at the no-flux boundary of the system to observe the stability of the wave train, and with a system size of 1000 μm. The temperature shift was increased in steps of 0.005 K.

The diagram contains three curves, separating the regimes of turbulence (found in both limits, for small and large ΔT), complete control, and partial control. For small ΔT, the heterogeneity is not strong enough to suppress turbulence. With increasing ΔT, we enter a regime of complete control. Here, the wave number and frequency of the created waves are large enough to suppress turbulence. As we will discuss in more detail below [Fig. 7(b)], the wavelength decreases as ΔT increases and complete control is replaced by partial control. Partial control becomes gradually weaker, i.e., suppresses turbulence in smaller areas around the heterogeneity, and gives way to turbulence for large ΔT. Thus, large temperature shifts do not necessarily result in better control. In general, no strong dependence on σ is observed. However, in the limit of small temperature heterogeneities (small σ) the curves are shifted toward larger values of ΔT, indicating that for those σ control is more difficult to obtain.

Within the domains of control, the wavelength decreases with increasing temperature shift for a given spot extension. This is shown for two examples in Fig. 7(b). Although for a small spot extension (solid curve), larger temperatures are necessary to control spatiotemporal chaos than for a large spot extension (dashed curve), the wavelengths of target waves that are able to suppress turbulence lie within the same range, approximately between 60 μm and 100 μm. This demonstrates that neither a specific temperature shift nor spot size is crucial to obtain control, as long as the wavelength of the created target waves lies in a particular, efficient range. For temperature heterogeneities creating waves with wavelengths larger than 100 μm, waves cannot suppress turbulence. The filled symbols represent simulations in the regime of partial control. The fact that wave trains become increasingly unstable as the wavelength decreases, supports the interpretation that the instability that provokes first the loss of complete and later also of partial control is related to the Eckhaus instability.

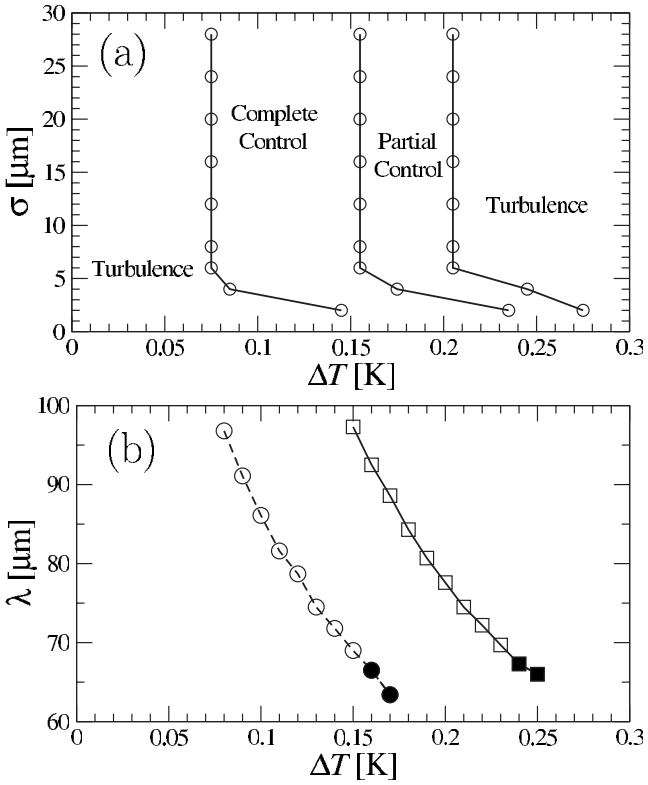

FIG. 7. Analysis of patterns induced by the pacemaker. (a) Control diagram. Depending on the choice of parameters ΔT (temperature shift) and σ (size of the heterogeneity) we find regions of partial and complete control. (b) Wavelength of the generated target patterns as a function of temperature shift for σ=2 μm (solid curve) and σ=24 μm (dashed curve). Solid symbols indicate simulations that lie in the regime of partial control.

It is helpful to comment on how the curves in Fig. 7(a) are obtained and on how they depend on initial conditions. First, the curve separating turbulence from complete control: Since uniform oscillations are stable and turbulence is intermittent, it is possible that turbulence decays spontaneously. Although this is very unlikely, in particular when the system size comprises more than a few wavelengths of the typical wave pattern, it is possible that some apparently turbulent initial conditions develop into uniform oscillations. Furthermore, it can be expected that the time necessary to observe control, diverges as the curve is reached. Hence, the position of the curve depends slightly on initial conditions and on the length of the simulation.

Second, the curve between the regimes of partial and complete control: Since the loss of complete control is related to the Eckhaus instability of traveling waves, which

develops and becomes manifest at a finite distance from the source of the traveling waves, the position of the numerically obtained curve depends slightly on the system size. If the system is too small, the curve moves to the right.

Third, the curve separating partial control from turbulence: As ΔT increases, the area filled with target waves decreases. However, at the wave source itself we will always observe induced oscillations. Therefore, it is practically impossible to distinguish a situation with partial control with a small target from a trivial local impact. This is aggravated by the intermittent nature of the turbulence which may allow a target pattern of fluctuating size. To recognize a simulation as an example of partial control, we have required that, on average, we observe at least one wavelength of the pattern. For small σ, we require waves to extend approximately 3σ. But there always remains some ambiguity in determining the border between partial control and turbulence. Since for small σ the temperature profile is resolved only poorly by the grid, the accuracy of the position of the curves decreases, although single simulations performed for smaller Δx demonstrate that the main behavior—the shift toward larger ΔT for small σ—is robust.

C. Control for other pressures

Until now, we have considered fixed values for the partial pressures, where for the given base temperature T_0 the system displays intermittent turbulence. There, we have seen how control is achieved varying size and magnitude of the temperature shift. In this section, we fix the latter and vary the partial pressures.

Figures 8(a) and 8(b) are obtained through two systematic series of simulations, one without heterogeneity (a), characterizing the underlying, native system dynamics (always starting with turbulent initial conditions), and the other with heterogeneity (b), examining whether a target pattern is formed or not. Since the resulting parameter regions are thin and elongated, we had to use a high resolution sampling of the pressures: Oxygen partial pressure was changed in steps of 1×10^{-6} mbar and the CO partial pressure in steps of 4×10^{-7} mbar.

First, we discuss the dynamical regimes in the absence of any heterogeneity, i.e., reactive (oxygen-covered) state, CO-covered state, turbulence and uniform oscillations [Fig. 8(a)]. For low partial pressures of oxygen and high pressures of CO, the system is in the steady state of uniform CO coverage, whereas for high partial pressures of oxygen and low pressures of CO, the system is in the reactive steady state (uniform oxygen coverage). We do not indicate areas of bistability of steady states (present in particular in the high pressure regimes) and do not resolve into monostable, excitable and subexcitable regimes systematically. Three curves confine the other two native dynamical regimes: Between the lower blue curve and the red dashed curve there is the region of uniform oscillations and between the red dashed curve and the upper blue curve we observe turbulence.

It is important to note that we always start from turbulent initial conditions. Since turbulent states may coexist with uniform oscillations (as already discussed above), another curve could be drawn here, separating the region of coexistence from the region where any initial condition leads to turbulence. However, since our aim is to study the suppression of turbulence, we always start from turbulent initial conditions and therefore do not obtain this curve.

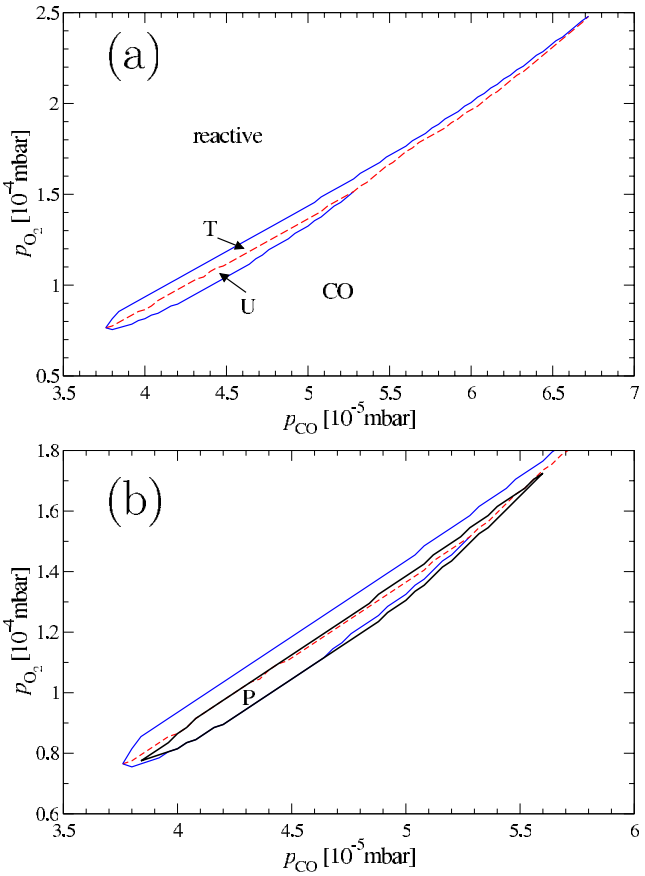

FIG. 8. (Color online) Diagram showing the main solutions of the CO oxidation system in the parameter space spanned by the partial pressures of oxygen and CO, without (a) and with (b) temperature heterogeneity. In (a), "*U*" denotes uniform oscillations, "*T*" denotes turbulence, "reactive" denotes the reactive-oxygen-covered state, and "CO" the CO-covered state. In (b), "*P*" denotes the area where the temperature heterogeneity constitutes a pacemaker, i.e., gives rise to target patterns. Where this area overlaps with the region "*T*" in (a), control of turbulence (complete or partial) is observed. For more information see text. The system size is $L=800$ μm and the simulation time is $t=2000$ s [and $t=8000$ s in the "*T*" region of (a)].

In Fig. 8(b), we superimpose on a part of Fig. 8(a) the region, limited by two black curves, where a temperature heterogeneity gives rise to a target pattern, starting with a turbulent initial condition. The fixed temperature heterogeneity is characterized by $\Delta T=0.15$ K and $\sigma=16$ μm. Whether this target pattern represents a case of control of turbulence depends on whether the underlying dynamics of the system are turbulent, consist of uniform oscillations, or are steady state. In the latter cases, target pattern formation proceeds as usual for oscillatory or excitable media, and the term "control of turbulence" is not applicable. In the remaining parameter space, the heterogeneity at most has a local impact and the global system behavior is ruled by the native dynamics.

In this picture, the region of control turns out to be a rather thin area, where the upper black curve lies above the red dashed curve. The main area where target patterns dominate lies in the part of parameter space where uniform oscillations are stable (in the region "*P*" below the red dashed curve and above the blue curve). There is also a thin region where target patterns are created although the medium is not oscillatory but excitable (when the lower black curve lies below the lower blue curve). For a large part of that area we have checked that the underlying dynamics are excitable with a steady state of high CO coverage as fixed point. We can also speculate that at least a part of the turbulent regime (toward high pressures) has underlying excitable rather than oscillatory dynamics. It is beyond the scope of this paper to check this rigorously.

Within the control regime, there is the small region of partial control in parameter space which is found adjacent to the turbulent regime. For low partial pressures, in the region between the red curve, the lower blue curve, and the black curves, the temperature heterogeneity is unable to create a target pattern on the background of stable oscillations. There, oscillations have a very small amplitude and no waves with a wavelength considerably smaller than the system size can be identified.

D. Dispersion relations

Until now, we have focused on the control aspect, i.e., on the ability of a temperature heterogeneity to suppress turbulence. In this section, we use the fact that we have a perfectly tunable wave source to determine the dispersion relations for the CO oxidation reaction for the parameters studied in Sec. III B.

Starting from unperturbed uniform oscillations as initial condition, even heterogeneities with small ΔT can initiate a target pattern although they would not be able to suppress turbulence. These target patterns are of longer wavelength than the ones we have observed under conditions of turbulence control. We can thus explore a wide range of ΔT values and measure the frequency and wavelength of the associated pattern. The results are shown in Fig. 9.

A typical way of characterizing oscillatory wave patterns is to measure the dependence of the frequency ω on the wave number k. In Fig. 9(a) we show that ω depends—to a good approximation—quadratically on k [a linear fit to $\omega=\omega(k^2)$ is shown], a feature also found for plane waves of generic models of oscillatory systems such as the complex Ginzburg-Landau equation (CGLE) or the simple phase dynamics equation [5]. We could in principle determine the parameters of the CGLE and the corresponding phase equation although we omit this here since we are not necessarily close to a Hopf bifurcation. Figure 9(b) displays the same data plotted as $\lambda(\tau)$, where τ denotes the period of the waves. As τ approaches the period of uniform oscillations, the wavelength diverges.

E. Control in the two-dimensional system

In the preceding sections, control of turbulence was systematically investigated for the one-dimensional KEE model

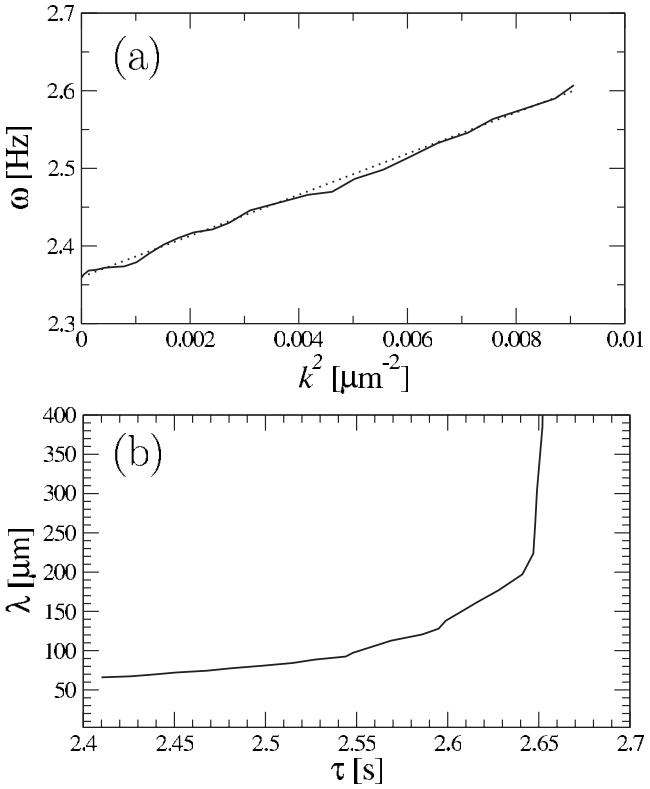

FIG. 9. Dispersion relations $\omega(k^2)$ (a) and $\lambda(\tau)$ (b). A linear fit to $\omega=\omega(k^2)$ (dotted curve) is added.

of catalytic CO oxidation. Here, we will extend this study to two spatial dimensions. As the computational costs for numerical simulations of the two-dimensional system are considerably higher than for the one-dimensional case, no systematic mapping of the control parameter space has been performed. Instead, we have carried out a number of coarse-grained parameter scans. They show, that the three different scenarios—turbulence, complete control, partial control—are also retained in the two-dimensional system. However, transients can be long and, in some cases, the states that are reached asymptotically showed sensitive dependence on the initial conditions.

Turbulence in two spatial dimensions proceeds along different lines than in one dimension, one fundamental reason being the existence of spiral cores acting as topological defects and organizing centers of spiral-wave chaos. We chose parameter values where turbulence was characterized by small interacting wave fragments.

In the following, we will present an example of complete control in the two-dimensional system. Parameters are chosen such that diffusion induced chemical turbulence spontaneously develops in the uniform system from random initial conditions. A snapshot of the spatiotemporally chaotic initial state is displayed in Fig. 10(a). At $t=0$ s, a temperature heterogeneity of Gaussian shape is initiated in the center of the computational domain. It is known that in two spatial dimensions heterogeneities with small extensions may be inefficient to emit waves [59] and hence we chose a relatively large σ. As in one dimension, the heterogeneity acts as a pacemaker that periodically emits concentric waves. In the

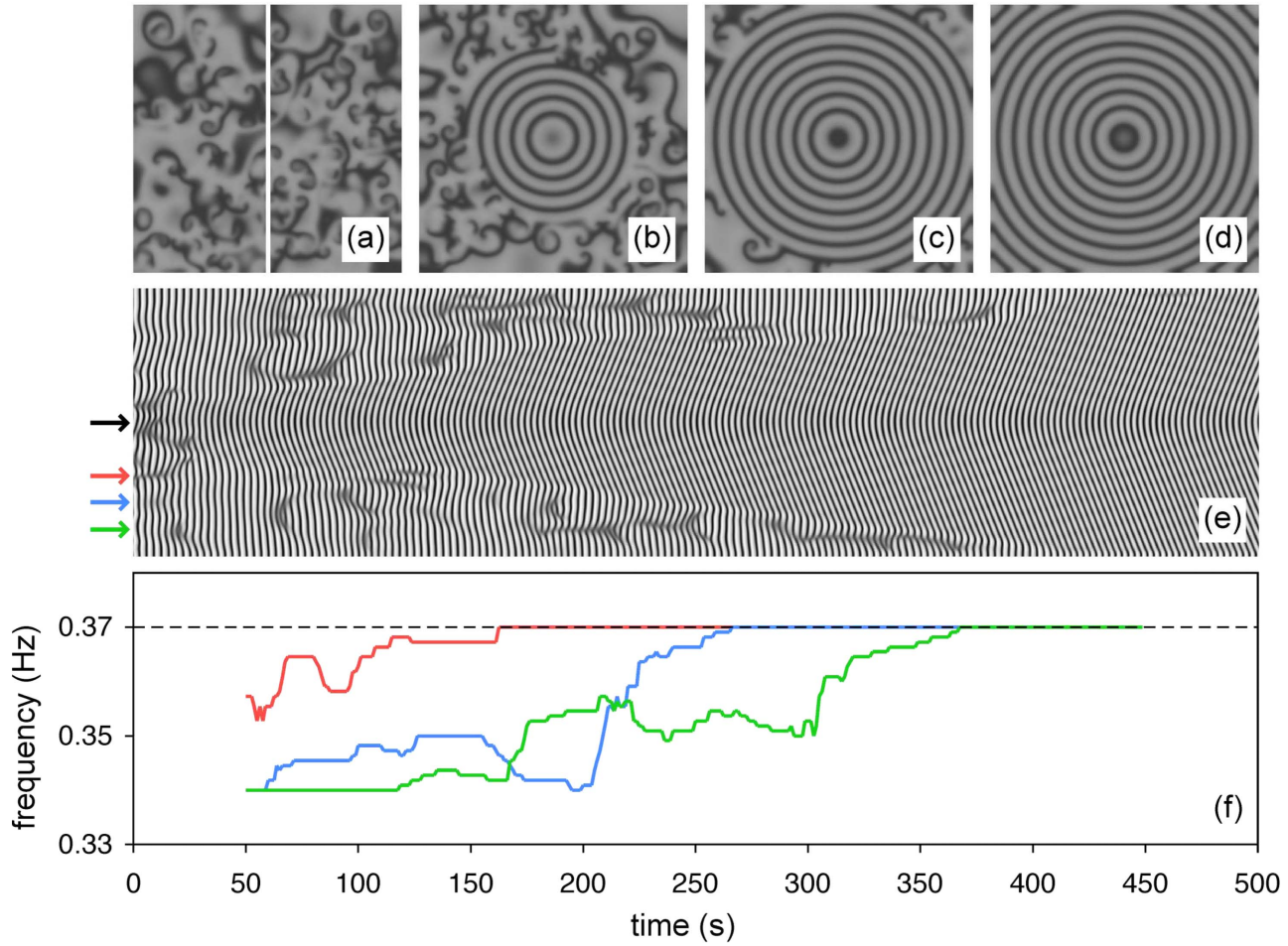

FIG. 10. (Color online) Control of chemical turbulence in a two-dimensional system by a temperature induced pacemaker. A temperature heterogeneity of Gaussian shape ($\Delta T=0.3$ K and $\sigma=40$ μm) is induced at $t=0$ s in the center of the domain. The partial pressures of the reactants are $p_{CO}=4.46\times10^{-5}$ mbar and $p_{O_2}=10.6\times10^{-5}$ mbar, the base temperature is $T_0=543.5$ K. (a) Chemical turbulence at time $t=0$ s. Emerging target pattern at (b) $t=250$ s, (c) $t=500$ s, and (d) $t=750$ s. (e) Space-time diagram along the vertical white line indicated in (a); time axis as in (f). (f) Frequency analysis of time series at four different points in space indicated by colored arrows on the left-hand side of the space-time diagram (e), the dashed black line shows the frequency in the center of the pacemaker.

course of time, the waves gradually invade the surrounding turbulent medium and a target pattern starts to emerge, see Fig. 10(b). After 500 s, the concentric waves fill already a large part of the medium, Fig. 10(c), and for longer times the entire system is entrained by the pacemaker, see Fig. 10(d) for $t=750$ s.

A space-time diagram is displayed in Fig. 10(e) to summarize the evolution of the system. It is taken along a vertical line through the center of the domain as indicated in Fig. 10(a). The concentric target waves are clearly distinct from the surrounding turbulent medium. As the target pattern grows, the chaotic domains are diminished until turbulence is completely suppressed at times beyond 500 s. We furthermore performed a frequency analysis of the temporal evolution at four different positions in the system, indicated by colored arrows on the left-hand side of Fig. 10(e). At each of these locations, time series from 11 adjacent pixels are considered. The frequency at each instant along a time series is determined from the maximal peak in the power spectrum, which is computed from a 100 s time interval centered around the considered point in time. For each of the four chosen locations, the frequency is then determined by averaging over the 11 adjacent time series. The results are shown in Fig. 10(f). The dashed black line represents the frequency at the center of the heterogeneity, and the colored lines correspond to locations indicated by the respective arrows.

Figure 10(f) clearly shows that the frequency at the center of the temperature heterogeneity is increased as compared to the colder parts of the system, as already shown above and in Ref. [38]. As the target pattern expands in the course of time, it reaches locations further away from the center of the domain, reflected in the successive increase in oscillation frequency at the red, blue, and green positions. Eventually, the entire medium is entrained by the pacemaker so that oscillations occur with identical frequencies across the whole system. This numerical result matches our experimental observations presented in Sec. II.

IV. SUMMARY

We have shown experimentally how turbulence in the oscillatory catalytic oxidation of CO on Pt(110) can be sup-

pressed through local control. By heating the surface of the platinum single crystal with focused laser light, we create a temperature heterogeneity which locally increases the system frequency. This constitutes a pacemaker in the system which emits concentric waves into the surrounding turbulent patterns and suppresses chemical turbulence.

Our experimental results are accompanied by a detailed numerical analysis of the KEE model for catalytic CO oxidation. In our one-dimensional simulations, we analyze how the degree of control and the spatiotemporal patterns that evolve in the system depend on control parameters such as the amplitude and width of the temperature heterogeneity. Furthermore, we investigate the system behavior for different global reaction parameters, i.e., different partial pressures of oxygen and CO. We find that in an area of parameter space where heterogeneous pacemakers exist and the system is in a turbulent state, control through the development of target patterns can be achieved. Additionally, in our simulations the temperature heterogeneity is used as a tool to determine the dispersion relation of the system. Numerical simulations in two spatial dimensions are conducted to complement the one-dimensional results and achieve a better comparability with the experimental section.

In the model calculations, the control parameters are chosen such that the dynamic regime without control and the observed behavior with control are qualitatively similar to the experiment. This means that we do not target a quantitative agreement between experiment and model calculations. In particular, a small ΔT is sufficient to obtain control in the model calculations, while in the experiment, the temperature heterogeneity needs to be sufficiently large to dominate over heterogeneities which are naturally present due to surface defects and fluctuations.

To summarize, we demonstrated experimentally that turbulence can be controlled in two-dimensional oscillatory systems through externally controlled pacemakers, and we find a qualitative agreement between the experiment and the results of numerical realistic model simulations. Besides complete control we find phase slip dynamics (related to partial control) both in simulation and experiment. While control of turbulence through pacemakers has been predicted in the CGLE [45], we believe that the present work shows, for the first time, experimental evidence for the viability of this method. The synchronization of dynamical systems through local heterogeneities leading to pacemakers is a simple and elegant approach which we expect to play an important role in other chemical, physical, or biological systems.

ACKNOWLEDGMENTS

One of the authors (M.S.) acknowledges support from European Commission (2003–2005) and INTA (2005–2007).

[1] G. Nicolis and I. Prigogine, *Self-Organization in Nonequilibrium Systems* (Wiley, New York, 1977).
[2] J. M. T. Thompson and H. B. Stewart, *Nonlinear Dynamics and Chaos* (Wiley, Chichester, 1986).
[3] M. C. Cross and P. C. Hohenberg, Rev. Mod. Phys. **65**, 851 (1993).
[4] Y. Kuramoto, *Chemical Oscillations, Waves, and Turbulence* (Springer, Berlin, 1984).
[5] A. S. Mikhailov, *Foundations of Synergetics I, Distributed Active Systems* (Springer, Berlin, 1994).
[6] J. D. Murray, *Mathematical Biology* (Springer, Berlin, 1989).
[7] I. R. Epstein and J. Pojman, *An Introduction to Nonlinear Chemical Dynamics* (Oxford University Press, New York, 1998).
[8] Z. Noszticzius, W. Horsthemke, W. D. McCormick, H. L. Swinney, and W. Y. Tam, Nature (London) **329**, 619 (1987).
[9] G. Ertl, Science **254**, 1750 (1991).
[10] R. Imbihl and G. Ertl, Chem. Rev. **95**, 697 (1995).
[11] S. Jakubith, H. H. Rotermund, W. Engel, A. von Oertzen, and G. Ertl, Phys. Rev. Lett. **65**, 3013 (1990).
[12] T. Engel and G. Ertl, Adv. Catal. **28**, 1 (1979).
[13] K. Krischer, M. Eiswirth, and G. Ertl, J. Chem. Phys. **96**, 9161 (1992).
[14] A. S. Mikhailov and K. Showalter, Phys. Rep. **425**, 79 (2006).
[15] B. A. Grzybowski and C. J. Campbell, Chem. Eng. Sci. **59**, 1667 (2004).
[16] L. Kuhnert, Nature (London) **319**, 393 (1986).
[17] V. Petrov, Q. Ouyang, and H. L. Swinney, Nature (London) **388**, 655 (1997).
[18] V. K. Vanag, L. Yang, M. Dolnik, A. M. Zhabotinsky, and I. R. Epstein, Nature (London) **406**, 389 (2000).
[19] T. Sakurai, E. Mihaliuk, F. Chirila, and K. Showalter, Science **296**, 2009 (2002).
[20] M. Kim, M. Bertram, M. Pollmann, A. von Oertzen, A. S. Mikhailov, H. H. Rotermund, and G. Ertl, Science **292**, 1357 (2001).
[21] M. Bertram, C. Beta, M. Pollmann, A. S. Mikhailov, H. H. Rotermund, and G. Ertl, Phys. Rev. E **67**, 036208 (2003).
[22] C. Beta, M. Bertram, A. S. Mikhailov, H. H. Rotermund, and G. Ertl, Phys. Rev. E **67**, 046224 (2003).
[23] C. Beta, M. G. Moula, A. S. Mikhailov, H. H. Rotermund, and G. Ertl, Phys. Rev. Lett. **93**, 188302 (2004).
[24] M. Bertram and A. S. Mikhailov, Phys. Rev. E **63**, 066102 (2001).
[25] M. Bertram and A. S. Mikhailov, Phys. Rev. E **67**, 036207 (2003).
[26] D. Battogtokh and A. S. Mikhailov, Physica D **90**, 84 (1996).
[27] D. Battogtokh, A. Preusser, and A. S. Mikhailov, Physica D **106**, 327 (1997).
[28] C. Beta and A. S. Mikhailov, Physica D **199**, 173 (2004).
[29] M. Bertram, C. Beta, H. H. Rotermund, and G. Ertl, J. Phys. Chem. B **107**, 9610 (2003).
[30] P. S. Bodega, P. Kaira, C. Beta, D. Krefting, D. Bauer, B. Mirwald-Schulz, C. Punckt, and H. H. Rotermund, New J. Phys. **9**, 61 (2007).
[31] J. Wolff, A. G. Papathanasiou, I. G. Kevrekidis, H. H. Rotermund, and G. Ertl, Science **294**, 134 (2001).
[32] J. Wolff, A. G. Papathanasiou, H. H. Rotermund, G. Ertl, M.

A. Katsoulakis, X. Li, and I. G. Kevrekidis, Phys. Rev. Lett. **90**, 148301 (2003).
[33] J. Wolff, A. G. Papathanasiou, H. H. Rotermund, G. Ertl, X. Li, and I. G. Kevrekidis, Phys. Rev. Lett. **90**, 018302 (2003).
[34] A. G. Papathanasiou, J. Wolff, I. G. Kevrekidis, H. H. Rotermund, and G. Ertl, Chem. Phys. Lett. **358**, 407 (2002).
[35] J. Wolff, A. G. Papathanasiou, H. H. Rotermund, G. Ertl, X. Li, and I. G. Kevrekidis, J. Catal. **216**, 246 (2003).
[36] L. Qiao, I. G. Kevrekidis, C. Punckt, and H. H. Rotermund, Phys. Rev. E **77**, 036214 (2008).
[37] J. Wolff and H. H. Rotermund, New J. Phys. **5**, 60 (2003).
[38] J. Wolff, M. Stich, C. Beta, and H. H. Rotermund, J. Phys. Chem. B **108**, 14282 (2004).
[39] L. Qiao, I. G. Kevrekidis, C. Punckt, and H. H. Rotermund, Phys. Rev. E **73**, 036217 (2006).
[40] L. Qiao, I. G. Kevrekidis, C. Punckt, and H. H. Rotermund, Phys. Rev. E **73**, 036219 (2006).
[41] H. G. Schuster and E. Schöll, *Handbook of Chaos Control* (Wiley-VCH, Weinheim, 2008).
[42] A. N. Zaikin and A. M. Zhabotinsky, Nature (London) **225**, 535 (1970).
[43] M. Stich, M. Ipsen, and A. S. Mikhailov, Phys. Rev. Lett. **86**, 4406 (2001).
[44] M. Stich, M. Ipsen, and A. S. Mikhailov, Physica D **171**, 19 (2002).
[45] M. X. Jiang, X. N. Wang, Q. Ouyang, and H. Zhang, Phys. Rev. E **69**, 056202 (2004).
[46] C. Beta, A. S. Mikhailov, H. H. Rotermund, and G. Ertl, Europhys. Lett. **75**, 868 (2006).
[47] M. Stich, C. Punckt, C. Beta, and H. H. Rotermund, Philos. Trans. R. Soc. London, Ser. A **366**, 419 (2008).
[48] J. Dicke, P. Erichsen, J. Wolff, and H. H. Rotermund, Surf. Sci. **462**, 90 (2000).
[49] C. Punckt, F. S. Merkt, and H. H. Rotermund, New J. Phys. **9**, 213 (2007).
[50] C. Punckt and H. H. Rotermund, Phys. Chem. Chem. Phys. **9**, 3635 (2007).
[51] M. Stich and A. S. Mikhailov, Z. Phys. Chem. **216**, 521 (2002).
[52] M. Bär, M. Hildebrand, M. Eiswirth, M. Falcke, H. Engel, and M. Neufeld, Chaos **4**, 499 (1994).
[53] M. van Hecke, Phys. Rev. Lett. **80**, 1896 (1998).
[54] M. Argentina and P. Coullet, Physica A **257**, 45 (1998).
[55] M. Argentina, O. Rudzick, and M. G. Velarde, Chaos **14**, 777 (2004).
[56] P. Coullet and L. Kramer, Chaos **14**, 244 (2004).
[57] Y. Hayase and H. R. Brand, J. Chem. Phys. **123**, 124507 (2005).
[58] N. Manz and O. Steinbock, Chaos **16**, 037112 (2006).
[59] M. Stich and A. S. Mikhailov, Physica D **215**, 38 (2006).